Journal of
Materials Chemistry B

PAPER

View Article Online
View Journal

Cite this: DOI: 10.1039/c5tb01199j

Fabrication of metal–organic single crystalline nanowires and reduced graphene oxide enhancement for an ultrasensitive electrochemical biosensor

Changhui Tan, Wuxiang Zhang, Jianzhong Zheng,* Xiuli You, Xuan Lin and Shunxing Li

Received 21st June 2015,
Accepted 5th August 2015

DOI: 10.1039/c5tb01199j

www.rsc.org/MaterialsB

A novel strategy is first presented here to design and construct a good selective and highly sensitive dopamine (DA) biosensor based on single-crystalline CuPc nanowires with a reduced graphene oxide–Nafion film (rGON/CuPcNWs). Metal–organic semiconductor single-crystalline CuPc nanowires with excellent electronic properties and large surface-to-volume ratios were prepared using a physical vapor transport technique and modified onto a glassy carbon electrode (GCE), and exhibited high electrocatalytic activity for DA detection by immobilizing it onto a GCE with a film of the rGON composite. The introduction of a rGO–Nafion film can significantly improve the electrochemical signal of the CuPcNWs. The relevant detection limit toward dopamine is 0.3 nM with a wide linear range from 0.001 μM to 200 μM. The results of the demonstrated biosensor could provide important enlightenment for the design of more sensitive electrochemical biosensors.

1. Introduction

Neurotransmitters, such as dopamine (DA), play a vital role in the functions of the central nervous, cardiovascular, endocrine, and renal systems. Abnormal dopaminergic neuron processes may lead to various neurological diseases.[1] Therefore, the rapid, low cost and effective detection of dopamine is very important in biological systems and meaningful for the routine diagnosis and analysis of neurological disorders.[2] To date, various methods of DA sensing have been reported. Among them, the electrochemical method for the determination of DA has been developed as a promising technique and has attracted much more attention owing to its high sensitivity and selectivity, operation simplicity, rapid response and low instrumental expenses.[3] It is important to fabricate a chemically modified electrode for the detection of DA with high selectivity and sensitivity. Hence, there are several works which report using modified nanomaterials such as metal nanoparticles,[4] quantum dots,[5] metal oxides,[6,7] carbon materials,[8,9] and conducting polymers[10,11] to improve the sensitivity, selectivity and stability of the modified electrode. However, physiological levels of DA range from nanomolar to low micromolar, and the current electrochemical sensors of DA are not only complicated due to their nanomaterial synthesis and sensor preparation, but also the current electrochemical sensors suffer from limited sensitivity and specificity toward DA. Thus, this creates a challenge for the preparation of highly sensitive and selective tools with very low detection limits to achieve the monitoring of DA for biological applications.[12]

More recently, metal–organic complexes, a novel class of hybrid materials constructed from metal-containing nodes connected by organic bridges, have garnered much more attention due to their useful applications in gas storage, separation, catalysis, sensing, and other technologies.[13–16] Metal-substituted phthalocyanines (MPcs), a fascinating class of metal–organic complexes, have gathered significant scientific interest, due to their excellent properties such as low cost and high conductivity. In previous studies, various metal–phthalocyanine powder composites have been applied as chemiresistive gas sensors[17,18] and biosensors,[19–23] because of their distinguished merits such as low cost, endurance, high sensitivity, high stability and good reliability. Nevertheless, the synthesis of single crystalline MPc nanowires, crystal metal–organic semiconductors with the remarkable property characteristics of organic–inorganic hybrid materials, is an important issue in materials science.[24] In addition, to the best of our knowledge, no prospective studies have reported the association of single crystalline MPc nanowires with biosensors. Recently, controlling single crystalline metal–organic semiconductor nanowires has been a challenging and significant

College of Chemistry and Environment, Fujian Province Key Laboratory of Morden Analytical Science and Separation Technology, Minnan Normal University, Zhangzhou 363000, P. R. China. E-mail: zhengjianzhong49@163.com; Fax: +86 596 2520035; Tel: +86 596 2591445

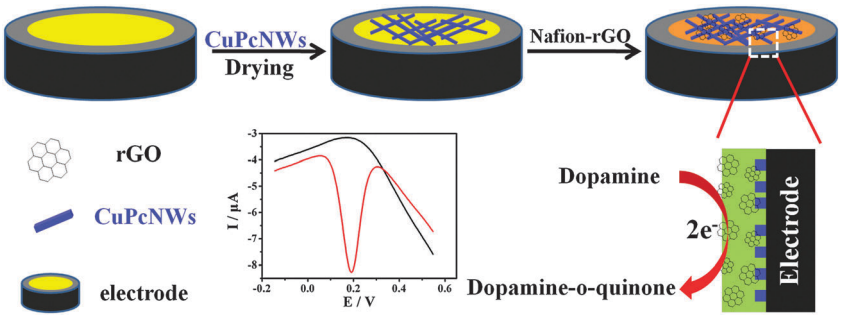

Scheme 1 Schematic of the CuPcNWs modified GCE with rGON composite film used for detecting DA.

objective owing to their novel properties and potential applications in the field of biosensing. Therefore, to fabricate a simple and high sensitivity electrochemical biosensor using single-crystalline metal–organic semiconductor nanowires would be desirable.

Herein, we chose single-crystalline copper phthalocyanine nanowires (CuPcNWs) to prepare large surface-to-volume ratios of nanowires, which were subsequently applied and combined with a film of rGON composite for the construction of a DA biosensor with a high electrochemical response efficiency (Scheme 1). The rGO can significantly enhance the electrical conductivity of the Nafion film, and hence improve the electrocatalytic activity of the single-crystalline CuPcNWs and affect their electrochemical response intensity. The biosensor revealed a highly sensitive and selective electrochemical response in a wide linear range with a low detection limit, when it was used for the detection of dopamine.

2. Experimental section

2.1. Reagents

Sodium nitrate, hydrochloric acid, hydrogen peroxide (30%), barium chloride, sulfuric acid and potassium permanganate were purchased from Shantou Xilong chemical Co., Ltd. Graphite powder was received from Sinopharm Chemical Regent. CuPc powder was bought from Alfa Aesar. Ascorbic acid, dopamine hydrochloride and uric acid were provided from Shanghai Sinopharm Chemical Reagent Co., Ltd. Nafion (5 wt%) was obtained from Sigma-Aldrich. Real samples (human serum and urine) were provided from Zhangzhou hospital. Human procedures were in agreement with the guidelines of the Nuremberg Code, Declaration of Helsinki, the Belmont Report and the regional ethics committee for human experiments. Human experiments were approved by the Zhangzhou Department of Health.

2.2. Characterization

The surface morphology of single-crystalline CuPc nanowires on silicon wafer was observed using a Japan Hitachi S4800 scanning electron microscope (SEM) at 10 kV. Transmission Electron Microscopy imaging (TEM) was carried out on a FEI Tecnai G2 S-TWIN operated at 200 kV. Scanning transmission electron microscopy (STEM) and selected area electron diffraction (SAED) were performed in an America FEI G2 F20 U-TWIN. The powder X-ray diffraction (XRD) pattern was recorded on a D/MAX-TTRIII (CBO) by using Cu Kα (λ = 1.54056 Å) radiation. Fourier transform infrared (FTIR) spectra were recorded on an America PE2000 in the spectral range of 500–4000 cm^{-1} using the KBr disk method. All electrochemical measurements were carried out on a Shanghai CHI660E electrochemical workstation with a three-electrode system consisting of Ag/AgCl, platinum wire and a glassy carbon electrode, serving as a reference electrode, counter electrode and working electrode, respectively.

2.3. Preparation of single-crystalline CuPcNWs and rGO

Single-crystalline CuPcNWs were thermally evaporated on Si wafers with a native oxide layer. Our strategy for the synthesis of a hybrid system is illustrated below. The formation of the experimental set-up of the CuPcNWs growth: a quartz tube was inserted in a tow-zone horizontal tube furnace. CuPc powder was placed and vaporized in the high temperature zone (450 °C) of the quartz tube in a tow-zone horizontal tube furnace with accurate temperature control. Vapor streams of CuPc molecules by sublimation were transported and deposited on the SiO_2 substrates in the 150 °C zone using an unchangeable Ar flowing method at a rate of 100 sccm. This process of sublimation was terminated after 3 hours. Purple fuzz-like CuPcNWs were obtained and observed on SiO_2 substrate after the setup was cooled to room temperature. Graphite oxide and rGO were prepared according to related literature methods.[25,26]

2.4. Preparation of the modified electrodes

Prior to use, the glassy carbon electrodes (GCEs) were polished on chamois leather with alumina (1.0 and 0.05 μm) slurry sequentially, and then washed ultrasonically in ethanol and water, respectively. The cleaned GCEs were dried at room temperature for the next modification. Then 5.0 μL of a solution of the CuPcNWs dispersion was applied onto the GCE surface and dried in air at room temperature. Then, a reduced graphene oxide–Nafion hybrid aqueous suspension was obtained by adding rGO of a different quality into 1 mL 0.5% Nafion diluent aqueous suspension and then sonicating for 30 min, which was cast onto the surface of CuPcNWs/GCE. The biosensor was obtained after being dried in the air.

3. Results and discussion

3.1. Characterization of single-crystalline CuPcNWs and rGO

The important features of the materials were characterized using microscopy and spectroscopy. A typical TEM image of rGO (Fig. 1A) exhibits the characteristic wrinkle and sheet structure. The SEM image of single-crystalline CuPcNWs (Fig. 1B) indicates that the obtained nanowires have a 1D wire-like structure. Without external force, the nanowires were straight. Fig. 1C shows the FT-IR spectra of CuPc powder and CuPcNWs in the spectral range of 500–4000 cm^{-1}. In the FT-IR spectrum of CuPc powder, the broad peak at 3430 cm^{-1} could be attributed to the O–H vibration of H_2O in the sample. The absorption bands of C=N and aromatic C=C were observed at 1630 and 730 cm^{-1} in the spectrum of the CuPc powder. In addition, one peak at around 1165 cm^{-1}, attributed to C–N can be clearly discerned. The result indicates that all the peaks of the CuPc powder could be fully retained in the CuPcNWs spectrum. Evidently, using the facile physical vapor transport technique is an effective way to prepare single-crystalline CuPcNWs. The X-ray diffraction powder pattern (Fig. 1D) of the CuPcNWs further confirms this conclusion and presents the dominance of [001] lattice planes in the case of the nanowires. The selected area electron diffraction (SAED) pattern of the CuPc nanowires reveals that CuPc nanowires are single crystalline in structure and grow along the [010] direction (Fig. 1E and F).

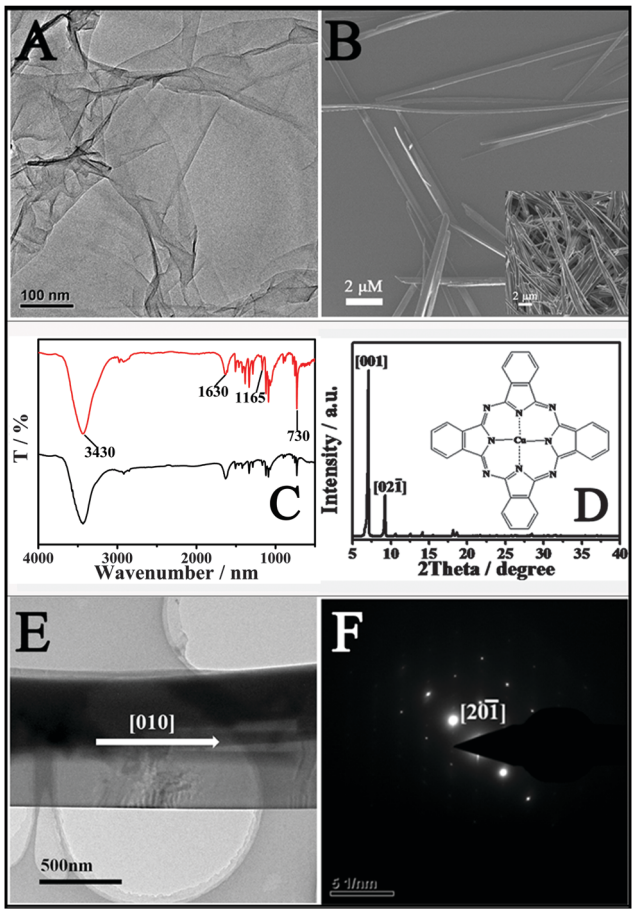

Fig. 1 (A) A TEM image of rGO exhibits the characteristic wrinkle and sheet structure. (B) A SEM image of the CuPcNWs, which shows the highly smooth surfaces and regular geometric shapes of the wires. (C) The Fourier transform infrared (FT-IR) spectra of CuPc powder and CuPcNWs. (D) XRD patterns of the CuPcNWs. Inset: Molecular structure of CuPc. (E) TEM image of a single wire. The arrow indicates the direction of the wire axis. (F) SAED pattern of the CuPcNWs.

3.2. Electrocatalysis of DA on the CuPcNWs-interface

A one-dimensional nanostructure can enhance the electrocatalytic reactivity and decrease the detection limit in the detection of an electrocatalytic reaction due to its large aspect ratio.[26,27] In terms of the electrochemical detection, the electrocatalytically active surface area of the electrode is helpful for enhancing the contact between the analyte and the electrochemical responses on the electrode, which plays an important role in improving the electroactivity of the electrode.[28,29] Therefore, it is an effective method to deposit high surface-to-volume ratios of single-crystalline CuPcNWs onto the surface of an electrode to obtain a large area interface.[30,31] The electrocatalytic activity of the modified electrodes were examined in 1 mM $[Fe(CN)_6]^{3-}$ solution containing 100 mM KCl for a reversible process, using cyclic voltammetry. As shown in Fig. 2, the electroactive surface area can be estimated according to the Randles–Sevcik equation:

$$I_p = 2.69 \times 10^5 A D^{1/2} n^{3/2} \nu^{1/2} C$$

where I_p is the peak current, A is the apparent electroactive surface area (cm^2), D is the diffusion coefficient of the reactant species in solution ($6.70 \pm 0.02 \times 10^{-6}$ cm^2 s^{-1} at 25 °C), n is the number of electrons participating in the reaction (for $[Fe(CN)_6]^{3-/4-}$, $n = 1$), ν is the scan rate (V s^{-1}), and C is the concentration of the reactant (a redox probe, $[Fe(CN)_6]^{3-/4-}$, mM). The electroactive surface area of the composite material (0.4964 cm^2) is about 7 times larger than that of the bare GCE electrode (0.07094 cm^2), indicating that the CuPcNWs could significantly increase the electroactive surface area of the electrode.

3.3. Optimization study of the rGON/CuPcNWs modified electrode

The CuPcNWs/GCE with a larger electroactive area could provide more binding sites for analytes compared with a bare GCE. As organic–inorganic semiconducting hybrid materials, CuPcNWs of a single composite have the potential benefit of integrating the functions of organic and inorganic components due to being built from linking metal ions and organic ligand connecting points. DA, as a small organic molecule could be successfully absorbed by using the organic linker of a metal–organic complex, and a transfer of electrons would take place from the organic ligand (phenyl group) to the metal ion (Cu^{2+}). However, the CuPcNWs may fall from the electrode surface if the electrode is modified directly by CuPcNWs, resulting in poor response stability followed by a decline in the current intensity (Fig. 3A).

To improve the stability of the CuPcNWs/GCE, Nafion film, which is one of the most popular materials to immobilize reagents, has been widely used for the modification of electrode

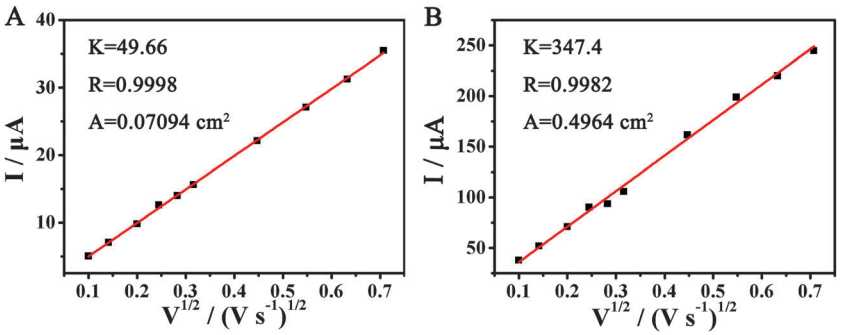

Fig. 2 Dependence of the anodic peak current of (A) the bare GCE and (B) the CuPcNWs/GCE against the square root of the scan rate.

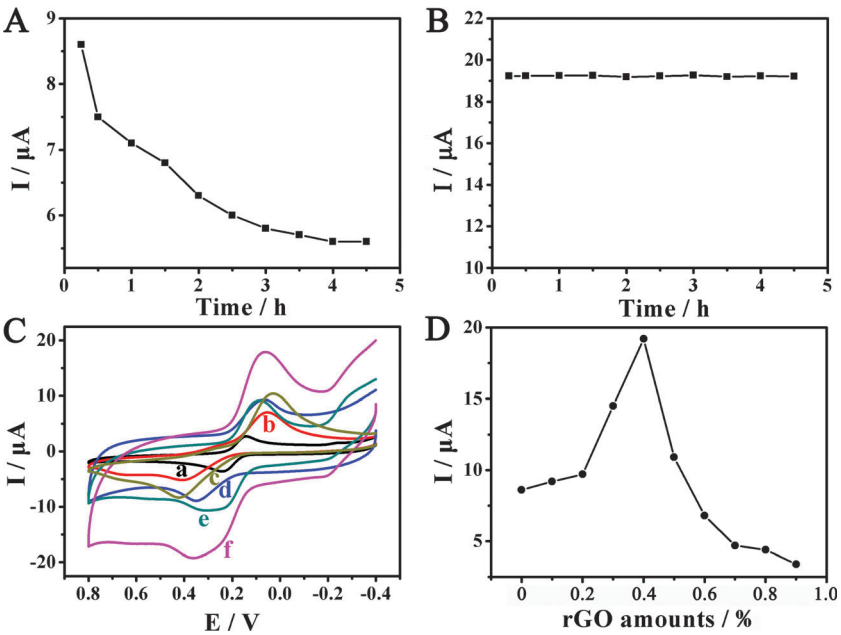

Fig. 3 Time dependent current intensities of the (A) CuPcNWs/GCE and (B) rGON/CuPcNWs/GCE on immersion into 0.1 mM DA 0.1 M pH 7.00 PBS. (C) CVs of (a) the GCE, (b) the Nafion/GCE, (c) rGON/CuPc powder/GCE, (d) the rGON/GCE, (e) the CuPcNWs/GCE, and (f) the rGON/CuPcNWs/GCE in 0.1 mM DA 0.1 M pH 7.00 PBS. Scan rate: 0.1 V s^{-1}. (D) Current intensities of the rGON/CuPcNWs/GCE as a function of the rGO doping ratio. The rGO concentration from left to right: 0%, 0.1%, 0.2%, 0.3%, 0.4%, 0.5%, 0.6%, 0.7%, 0.8% and 0.9%.

surfaces and for the construction of sensors.[32] Therefore, Nafion film was used to immobilize the CuPcNWs onto the electrode surface. Fig. 3B reveals that the current intensity of the rGON/CuPcNWs/GCE undergoes little change after a long immersion time when the rGON/CuPcNWs/GCE was immersed into PBS solution. The result illustrates that the CuPcNWs could be fixed and the storage time could be extended. Nevertheless, proton conductivity significantly declined after adding the Nafion solution. Herein, the electronic material rGO with outstanding physical and chemical properties[33–35] was mixed into the Nafion matrix to enhance its proton conductivity and facilitate the charge transfer, on account of the excellent conductivity of the two-dimensional planar structure of rGO. The CVs of the different materials modified electrodes were investigated. Fig. 3C demonstrates that the rGO could enhance the electrocatalytic activity of the CuPcNWs, which results from the fact that rGO has an especially good charge transfer rate. The effect of the rGO with doping ratio on the electrocatalytic activity for optimizing the electrocatalytic properties of rGON/CuPcNWs/GCE was systematically investigated. Fig. 3D shows the dependence of the current response intensities on the rGO content. The current intensity increases significantly with the doping ratio of rGO up to a maximum at 0.4%, while it then decreases with a further rise in the rGO content in the Nafion film. The increase in the rGO doping ratio leads to an enhancement of the current response intensity. It is interesting to observe that the proton conductivity of the Nafion-based film is enhanced when 0.4% of rGO is introduced in the Nafion matrix, because rGO could help in the formation of a better network channel for proton transport. When the rGO content was below 0.4%, the film impeded electron conduction and π–π interaction between rGO and the DA molecules due to the small amounts of rGO that could be completely covered in the Nafion film. However, further increasing the rGO content above 0.4%,

the rGO aggregates and weakens the electrostatic interaction of the electronegative rGO–Nafion film with the positively charged DA.

3.4. Electrochemical parameters of DA at rGON/CuPcNWs/GCE

The influence of scan rates (ν) on the electrochemical response of rGON/CuPcNWs/GCE in 0.1 mM DA 0.1 M pH 7.00 PBS was examined by varying the scan rates from 0.01 to 0.5 V s^{-1} (Fig. 4A). Upon increasing the scan rate, both the anodic and cathodic peak currents increased gradually, yet the anodic and cathodic peak potentials slightly shifted to more positive and negative potentials respectively, and a good linear dependence of the redox peak currents on the scan rate was obtained (Fig. 4B); linear regression equations (R_{pa} = 0.9945 and R_{pc} = 0.9976):

$$I_{pa}\ (\mu A) = 5.03313 + 0.11027\nu\ (V\ s^{-1})$$

$$I_{pc}\ (\mu A) = -5.96747 - 0.12254\nu\ (V\ s^{-1})$$

In addition, as for a quasi-reversible adsorption-controlled process, the number of electrons (n) and the electron transfer coefficient (α) can be acquired according to Laviron's equation:

$$E_{pa} = E^{0'} + \frac{2.3RT}{(1-\alpha)nF}\log\nu \quad (1)$$

$$E_{pc} = E^{0'} - \frac{2.3RT}{\alpha nF}\log\nu \quad (2)$$

where E_{pa} and E_{pc} are the oxidation and reduction peak potentials, respectively, R is the ideal gas constant, T is the temperature and F is Faraday's constant. The linear dependence for DA between the redox peak potentials and $\log\nu$ can be found at scan rates from 0.01 to 0.5 V s^{-1} where E_{pa}/V = 0.4904 + 0.06580 × $\log\nu$ (V s^{-1}) (R = 0.9964), E_{pc}/V = −0.00143 − 0.06073 × $\log\nu$ (V s^{-1}) (R = 0.9957), and then n was calculated to be 1.89, indicating a two-electron and two-proton process at the biosensor interface consistent with the results in the literature.[21] Moreover, α was estimated to be 0.52, which is close to the theoretical value of 0.5 for a quasi-reversible process.

3.5. Calibration plot and limit of detection

Voltammetric current responses of successive additions of DA were recorded by DPV to check the sensitivity of the biosensor due to its higher sensitivity and minimization of any noise from stirring. As shown in Fig. 5A, are DPV curves of various concentrations of DA at rGON/CuPcNWs/GCE. Under optimal conditions, the oxidation peak current (I_{pa}) of DA increased linearly with the increase of DA concentration in the range from 0.001 μM to 25 μM and 25 μM to 200 μM (inset of Fig. 5A), with linear regression equations of I_{pa} (μA) = −0.165C (μM) − 3.226 (R_1 = 0.9981) and I_{pa} (μA) = −0.0333C (μM) − 6.4587 (R_2 = 0.9975). The limit of detection was estimated to be 0.3 nM based on a S/N of 3 and the relative standard derivation (RSD, n = 5) was less than 1.98%, which is sensitive enough for analyzing dopamine levels in many biological systems.[22] Furthermore, specificity is another important factor to evaluate a biosensor. In biological samples that contain DA, a variety of common biological interfering molecules also exists and several kinds of inorganic ions, especially ascorbic acid and uric acid, which exhibit similar redox behaviors to DA and hence can obscure the DA signal. To verify this, we investigated the DPV of the solution with continuous additions of 2 μM DA, 200 μM AA, and 200 μM UA. Fig. 5B shows that no signal increase was observed after continuous addition of ascorbic acid and uric acid. Here, a possible reaction mechanism is discussed. It is well known that Nafion is negatively charged in PBS (pH = 7.4) solution.[36] In addition, it has been reported in our previous study that DA (pK_a = 8.9) exists as a cation, UA (pK_a = 3.9) and AA (pK_a = 4.1) as an anion in PBS (pH = 7.4) solution.[4] Therefore, the rGON film not only could effectively repel the interference from the anionic electroactive substances (AA and UA), but could attract the positively charged DA analyte by electrostatic interactions and ion-exchange effects, which consequently improve the selectivity towards DA[37] detection. Moreover, oxidation signals that were unchanged could be observed in the presence of all of the interferences, such as glucose, L-cysteine (100-fold concentrations), Cl^-, NO_3^-, CO_3^{2-}, SO_4^{2-}, NH_4^+, K^+, Na^+, and Ca^{2+} (200-fold concentrations). It is clear that the developed electrochemical biosensor here could be applied for the sensitive detection of DA with high specificity. In addition, the performances of rGON/CuPcNWs biosensor were compared to the other types of DA biosensors (Table 1). The rGON/CuPcNWs biosensor shows a simple, higher sensitivity and selectivity, low cost, and high sensitivity than the other types of biosensors.

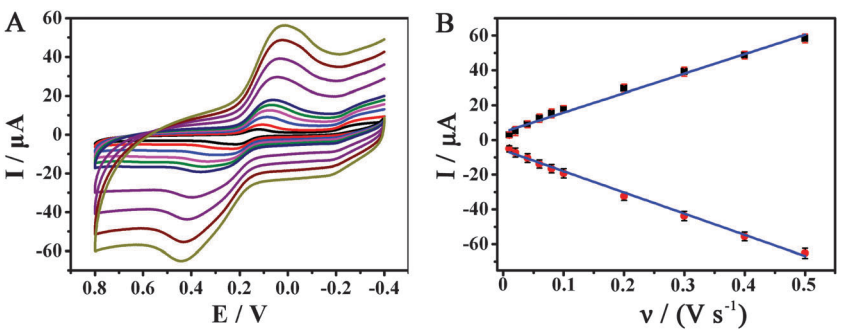

Fig. 4 (A) CVs of rGON/CuPcNWs/GCE in 0.1 mM pH 7.0 PBS containing 0.1 mM DA at different scan rates of 0.01, 0.02, 0.04, 0.06, 0.08, 0.1, 0.2, 0.3, 0.4 and 0.5 V s^{-1} (from inside to outside). (B) The plots of anodic and cathodic peak currents *vs.* scan rates.

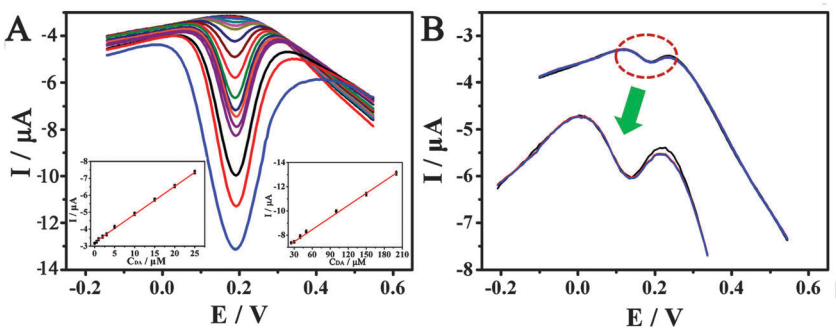

Fig. 5 (A) DPV for different concentrations of DA at rGON/CuPcNWs in 0.1 M PBS with pH 7.0 (scan rate: 0.1 V s^{-1}). The total concentration of DA in each step (from top to bottom: 0, 0.001, 0.5, 1, 2, 3, 5, 10, 15, 20, 25, 30, 40, 50, 100, 150 and 200 μM). Inset: The calibration plot of oxidation peak current *vs.* accumulated concentration of DA in each step. (B) DPV of modified electrodes with successive addition of 2 μM DA (black line), 200 μM AA (red line), and 200 μM UA (blue line).

Table 1 Comparison of the performance of various dopamine biosensors

Electrode materials	Linear range (μM)	Detection limit (nM)	Real-time detection	Ref.
Pt/graphene	0.03–8.13	30	No	6
N-PCNPs	0.5–30	11	No	7
Fe_3O_4/rGO	0.4–160	80	No	21
Pd NPs/graphene/chitosan	0.5–200	100	No	22
Cu_2O/graphene	0.1–10	10	No	23
Au@polymer	0.02–0.54	7.8	Yes	38
Au/Pt/Pd/TiO_2 NTs	0.05–30	30	Yes	39
Au@SiO_2-MIPs	0.048–50	20	Yes	40
Polypyrrole@rGO	0.06–8	6	No	41
LDH/CoPcTs	20–140	320	No	42
SiO_2/C/CuPc	10–140	600	No	43
MIPs-OAP–gold	0.02–0.25	1.98	No	44
Nafion–rGO/CuPcNWs	0.001–200	0.3	Yes	This work

Note: PCNPs = porous carbon nanopolyhedra, MIPs = molecularly imprinted polymers, MIPs-OAP = molecularly imprinted polymers-*o*-aminophenol.

3.6. Reproducibility and stability of the rGON/CuPcNWs electrode

The reproducibility and stability of the rGON/CuPcNWs modified electrode were studied. The relative standard deviation (RSD) of repeated DPV experiments with 1.0×10^{-6} M DA was examined under the optimal conditions, which was about 2.36% after 11 successive measurements were obtained indicating that the rGON/CuPcNWs modified electrode has an excellent reproducibility. The long-term stability of the rGON/CuPcNWs modified electrode was evaluated by measuring its DPV response to 1.0×10^{-6} M DA in 0.1 M pH 7.00 PBS and then repeating the same experiment after one month. The electrode was stored at room temperature under normal conditions when not in use. The oxidation current response maintained 98.49% of the original peak current value after one month, indicating the good stability of the fabricated electrode. These results indicate that rGON/CuPcNWs can be used as an advanced platform of high performance biosensors including a wide linear range, low detection potential, high sensitivity, excellent reproducibility, and good stability.

Table 2 Determination of DA levels in real samples using the rGON/CuPcNWs and DPV in 0.1 M PBS (pH 7.0)

Sample	Detected (μM)	Addition (μM)	Found (μM)	Recovery (%)	RSD (%)
Serum 1	—	5	5.0 ± 0.2	101.0	2.07
		10	9.9 ± 0.3	99.4	1.27
		15	15.0 ± 0.3	100.5	1.04
Serum 2	0.006	5	5.1 ± 0.2	101.5	2.46
		10	10.1 ± 0.2	101.1	1.48
		15	15.0 ± 0.3	100.4	0.89
Urine 1	1.2	5	5.1 ± 0.3	101.6	2.34
		10	10.0 ± 0.2	99.9	0.76
		15	15.0 ± 0.2	100.0	0.71
Urine 2	0.7	5	5.0 ± 0.1	99.8	1.94
		10	10.0 ± 0.1	100.3	0.77
		15	15.0 ± 0.2	101.2	0.99

3.7. Determination of DA in real human samples

To investigate the potential application of the rGON/CuPcNWs modified electrode, the standard addition method as a useful tool was carried out for the detection in real human samples. All of the real human samples were diluted 5 times with 0.1 M PBS (pH 7.0) before measurement. Then, different amounts of known concentrations of DA were added to the sample to obtain the appropriate concentrations. Table 2 represents the obtained results for five measurements. The recoveries of the spiked sample ranged between 99.4% and 101.6%, indicting the potential of the method is good enough for analyzing dopamine level in clinical applications.

4. Conclusions

In summary, we prepared single-crystalline CuPcNWs using a physical vapor transport technique, and immobilized them onto a GCE using a rGON composite film to fabricate a highly sensitive and selective electrochemical DA biosensor for the first time. The nanostructure of the single-crystalline CuPcNWs improved the properties of the electrochemical biosensor, due

to the amplified electroactive surface area of the electrode. Nafion film can not only prevent the single-crystalline CuPcNWs from dispersing into the electrolyte, but also improve the selectivity of the DA biosensor due to the electrostatic interaction between the film and analytes. By utilizing a composite film by the incorporation of rGO into Nafion to enhance the response and detection limit as a result of the rGO, can improve the conductivity of the film. This biosensor with Nafion–(0.4%) rGO showed a low detection limit down to 0.3 nM, a wide linear response range from 0.001 μM to 200 μM and excellent selectivity for DA. The prepared electrochemical biosensor has a remarkable detection performance, which could spur its further use in biosensing applications. The electrochemical intensity and stability of the single-crystalline CuPcNWs could promote the application of nanometre-sized materials in fabricating biosensors for chemical and biochemical analysis.

Acknowledgements

This work is supported financially by the NNSF of China (No. 21475055 and 21175115), the Program for New Century Excellent Talents in University (NCET-110904), and the Science and Technology Support Projects of Fujian Province (JA12218).

References

1 T. S. Tang, X. Chen, J. Liu, I. J. Bezprozvanny and J. E. Ahlskog, Beating a dead horse: dopamine and Parkinson disease, *Neurology*, 2007, **69**, 1701–1711.
2 S. R. Laviolette, Dopamine modulation of emotional processing in cortical and subcortical neural circuits: evidence for a final common pathway in schizophrenia?, *Schizophr. Bull.*, 2007, **33**, 971–981.
3 R. B. Keithley, P. Takmakov, E. S. Bucher, A. M. Belle, C. A. Owesson-White, J. Park and R. M. Wightman, Higher sensitivity dopamine measurements with faster-scan cyclic voltammetry, *Anal. Chem.*, 2011, **83**, 3563–3571.
4 W. X. Zhang, J. Z. Zheng, C. H. Tan, X. Lin, S. H. Hu, J. H. Chen, X. L. You and S. X. Li, Designed self-assembled hybrid Au@CdS core–shell nanoparticles with negative charge and their application as highly selective biosensors, *J. Mater. Chem. B*, 2015, **3**, 217–224.
5 P. M. Ndangili, O. A. Arotiba, P. G. Baker and E. I. Iwuoha, A potential masking approach in the detection of dopamine on 3-mercaptopropionic acid capped ZnSe quantum dots modified gold electrode in the presence of interferences, *J. Electroanal. Chem.*, 2010, 77–81.
6 C. L. Sun, H. H. Lee, J. M. Yang and C. C. Wu, The simultaneous electrochemical detection of ascorbic acid, dopamine, and uric acid using graphene/size-selected Pt nanocomposites, *Biosens. Bioelectron.*, 2011, **26**, 3450–3455.
7 P. B. Gai, H. J. Zhang, Y. S. Zhang, W. Liu, G. B. Zhu, X. H. Zhang and J. H. Chen, Simultaneous electrochemical detection of ascorbic acid, dopamine and uric acid based on nitrogen doped porous carbon nanopolyhedra, *J. Mater. Chem. B*, 2013, **1**, 2742–2749.
8 Z. Wang, J. Liu, Q. L. Liang, Y. Wang and G. Luo, A selective voltammetric method for uric acid detection at β-cyclodextrin modified electrode incorporating carbon nanotubes, *Analyst*, 2002, **127**, 653–658.
9 C. F. Wang, P. P. Xu and K. L. Zhuo, Ionic liquid functionalized graphene-based electrochemical biosensor for simultaneous determination of dopamine and uric acid in the presence of ascorbic acid, *Electroanalysis*, 2014, **26**, 191–198.
10 C. L. Weaver, H. Li, X. Luo and X. T. Cui, A graphene oxide/conducting polymer nanocomposite for electrochemical dopamine detection: origin of improved sensitivity and specificity, *J. Mater. Chem. B*, 2014, **2**, 5209–5219.
11 L. Sasso, A. Heiskanen, F. Diazzi, M. Dimaki, J. Castillo-León, M. Vergani, E. Landini, R. Raiteri, G. Ferrari, M. Carminati, M. Sampietro, W. E. Svendsen and J. Emnéus, Doped overoxidized polypyrrole microelectrodes as sensors for the detection of dopamine released from cell populations, *Analyst*, 2013, **138**, 3651–3659.
12 D. L. Robinson, A. Hermans, A. T. Seipel and R. M. Wightman, Monitoring rapid chemical communication in the brain, *Chem. Rev.*, 2008, **108**, 2554–2584.
13 L. J. Murray, M. Dinca and J. R. Long, Hydrogen storage in metal–organic frameworks, *Chem. Soc. Rev.*, 2009, **38**, 1294–1314.
14 J. R. Li, R. J. Kuppler and H. C. Zhou, Selective gas adsorption and separation in metal–organic frameworks, *Chem. Soc. Rev.*, 2009, **38**, 1477–1504.
15 J. Lee, O. K. Farha, J. Roberts, K. A. Scheidt, S. T. Nguyen and J. T. Hupp, Metal–organic framework materials as catalysts, *Chem. Soc. Rev.*, 2009, **38**, 1450–1459.
16 A. C. McKinlay, R. E. Morris, P. Horcajada, G. Ferey, R. Gref, P. Couvreur and C. Serre, BioMOFs: metal–organic frameworks for biological and medical applications, *Angew. Chem., Int. Ed.*, 2010, **49**, 6260–6266.
17 F. I. Bohrer, C. N. Colesniuc, J. Park, M. E. Ruidiaz, I. K. Schuller, A. C. Kummel and W. C. Trogler, Comparative Gas Sensing in Cobalt, Nickel, Copper, Zinc, and Metal-Free Phthalocyanine Chemiresistors, *J. Am. Chem. Soc.*, 2009, **131**, 478–485.
18 W. G. Huang, K. Besar, R. LeCover, A. M. Rule, P. N. Breysse and H. E. Katz, Highly sensitive NH_3 detection based on organic field-effect transistors with tris (pentafluorophenyl) borane as receptor, *J. Am. Chem. Soc.*, 2012, **134**, 14650–14653.
19 L. F. Chen, H. Y. Zheng, X. Zhu, Z. Y. Lin, L. H. Guo, B. Qiu, G. N. Chen and Z. N. Chen, Metal–organic frameworks-based biosensor for sequence-specific recognition of double-stranded DNA, *Analyst*, 2013, **138**, 3490–3493.
20 P. Kumar, L. M. Bharadwaj, A. K. Paul and A. Deep, Luminescent nanocrystal metal organic framework based biosensor for molecular recognition, *Inorg. Chem. Commun.*, 2014, **43**, 114–117.
21 H. Teymourian, A. Salimi and S. Khezrian, Fe_3O_4 magnetic nanoparticles/reduced graphene oxide nanosheets as a

novel electrochemical and bioelectrochemical sensing platform, *Biosens. Bioelectron.*, 2013, **49**, 1–8.

22 X. Wang, M. Wu, W. R. Tang, Y. Zhu, L. W. Wang, Q. J. Wang, P. A. He and Y. Z. Fang, Simultaneous electrochemical determination of ascorbic acid, dopamine and uric acid using a palladium nanoparticle/graphene/chitosan modified electrode, *J. Electroanal. Chem.*, 2013, **695**, 10–16.

23 F. Y. Zhang, Y. J. Li, Y. E. Gu, Z. H. Wang, Z. H. Wang and C. M. Wang, Non-enzymatic electrochemical sensing of glucose, *Microchim. Acta*, 2011, **173**, 103–109.

24 C. R. Kagan, D. B. Mitzi and C. D. Dimitrakopoulos, Organic–Inorganic Hybrid Materials as Semiconducting Channels in Thin-Film Field-Effect Transistors, *Science*, 1999, **286**, 945–947.

25 S. X. Li, J. Z. Zheng, D. J. Chen, Y. j. Wu, W. X. Zhang, F. Y. Zheng, J. Cao and Y. L. Liu, Yolk–shell hybrid nanoparticles with magnetic and pH-sensitive properties for controlled anticancer drug delivery, *Nanoscale*, 2013, **5**, 11718–11724.

26 Y. K. Che, X. M. Yang, S. Loser and L. Zang, Expedient vapor probing of organic amines using fluorescent nanofibers fabricated from an n-type organic semiconductor, *Nano Lett.*, 2008, **8**, 2219–2223.

27 K. Balakrishnan, A. Datar, R. Oitker, H. Chen, J. M. Zuo and L. Zang, Nanobelt self-assembly from an organic n-type semiconductor: propoxyethyl-PTCDI, effect of side-chain substituents on self-assembly of perylene diimide molecules: morphology control, *J. Am. Chem. Soc.*, 2005, **127**, 10496–10497.

28 J. Yu, F. R. Fan, S. Pan, V. M. Lynch, K. M. Omer and A. J. Bard, Spontaneous formation and electrogenerated chemiluminescence of tris (bipyridine) Ru(II) derivative nanobelts, *J. Am. Chem. Soc.*, 2008, **130**, 7196–7197.

29 J. Suk, Z. Wu, L. Wang and A. J. Bard, Electrochemistry, Electrogenerated Chemiluminescence, and Excimer Formation Dynamics of Intramolecular π-Stacked 9-Naphthylanthracene Derivatives and Organic Nanoparticles, *J. Am. Chem. Soc.*, 2011, **133**, 14675–14685.

30 C. Guo, F. Hu, C. M. Li and P. K. Shen, Direct electrochemistry of hemoglobin on carbonized titania nanotubes and its application in a sensitive reagentless hydrogen peroxide biosensor, *Biosens. Bioelectron.*, 2008, **24**, 819–824.

31 L. L. Li, K. P. Liu, G. H. Yang, C. M. Wang, J. R. Zhang and J. J. Zhu, Fabrication of graphene–quantum dots composites for sensitive electrogenerated chemiluminescence immunosensing, *Adv. Funct. Mater.*, 2011, **21**, 869–878.

32 Z. H. Guo and S. J. Dong, Electrogenerated chemiluminescence from Ru $(Bpy)_3^{2+}$ ion-exchanged in carbon nanotube/perfluorosulfonated ionomer composite films, *Anal. Chem.*, 2004, **76**, 2683–2688.

33 K. Si, R. Wycisk, D. Dong, K. Cooper, M. Rodgers, P. Brooker, D. Slattery and M. Litt, Rigid-rod poly-(phenylenesulfonic acid) proton exchange membranes with cross-linkable biphenyl groups for fuel cell applications, *Macromolecules*, 2013, **46**, 422–433.

34 F. Kim, L. J. Cote and J. X. Huang, Graphene oxide: surface activity and two-dimensional assembly, *Adv. Mater.*, 2010, **22**, 1954–1958.

35 C. F. Wang, Y. J. Chen, K. L. Zhuo and J. J. Wang, Simultaneous reduction and surface functionalization of graphene oxide *via* an ionic liquid for electrochemical sensors, *Chem. Commun.*, 2013, **49**, 3336–3338.

36 K. A. Mauritz and R. B. Moore, State of understanding of Nafion, *Chem. Rev.*, 2004, **104**, 4535–4585.

37 C. Z. Liao, M. Zhang, L. Y. Niu, Z. J. Zheng and F. Yan, Organic electrochemical transistors with graphene-modified gate electrodes for highly sensitive and selective dopamine sensors, *J. Mater. Chem. B*, 2014, **2**, 191–200.

38 C. Xue, Q. Han, Y. Wang, J. H. Wu, T. T. Wen, R. Y. Wang, J. L. Hong, X. M. Zhou and H. J. Jiang, Amperometric detection of dopamine in human serumby electrochemical sensor based on gold nanoparticles doped molecularly imprinted polymers, *Biosens. Bioelectron.*, 2013, **49**, 199–203.

39 S. Mahshid, C. C. Li, S. S. Mahshid, M. Askari, A. Dolati, L. X. Yang, S. L. Luo and Q. Y. Cai, Sensitive determination of dopamine in the presence of uric acid and ascorbic acid using TiO_2 nanotubes modified with Pd, Pt and Au nanoparticles, *Analyst*, 2011, **136**, 2322–2329.

40 D. J. Yu, Y. B. Zeng, Y. X. Qi, T. S. Zhou and G. Y. Shi, A novel electrochemical sensor for determination of dopamine based on AuNPs@SiO_2 core–shell imprinted composite, *Biosens. Bioelectron.*, 2012, **38**, 270–277.

41 T. Qian, S. S. Wu and J. Shen, Facilely prepared polypyrrole-reduced graphite oxide core–shell microspheres with high dispersibility for electrochemical detection of dopamine, *Chem. Commun.*, 2013, **49**, 4610–4612.

42 J. B. Han, X. Y. Xu, X. Y. Rao, M. Wei, D. G. Evans and X. Duan, Layer-by-layer assembly of layered double hydroxide/cobalt phthalocyanine ultrathin film and its application for sensors, *J. Mater. Chem.*, 2011, **21**, 2126–2130.

43 A. Rahim, S. B. A. Barros, L. T. Kubota and Y. Gushikem, SiO_2/C/Cu(II) phthalocyanine as a biomimetic catalyst for dopamine monooxygenase in the development of an amperometric sensor, *Electrochim. Acta*, 2011, **56**, 10116–10121.

44 J. P. Li, J. Zhao and X. P. Wei, A sensitive and selective sensor for dopamine determination based on a molecularly imprinted electropolymer of *o*-aminophenol, *Sens. Actuators, B*, 2009, **140**, 663–669.

